Atmos. Meas. Tech. Discuss., 3, 5907–5931, 2010
www.atmos-meas-tech-discuss.net/3/5907/2010/
doi:10.5194/amtd-3-5907-2010

Atmospheric Measurement Techniques Discussions

Characterization of a new fast mixing type CPC and its application for atmospheric particle measurements

B. Wehner, H. Siebert, M. Hermann, F. Ditas, and A. Wiedensohler

Leibniz Institute for Tropospheric Research, 04318 Leipzig, Germany

Received: 13 December 2010 – Accepted: 15 December 2010 – Published: 21 December 2010

Correspondence to: B. Wehner (birgit@tropos.de)

Published by Copernicus Publications on behalf of the European Geosciences Union.

Abstract

A new fast mixing-type CPC (FCPC) has been built based on the setup described by Wang et al. (2002). The functionality and stable operation of the FCPC was demonstrated in the laboratory as well as under atmospheric conditions. The counting efficiency was measured while the temperature difference between FCPC saturator and condenser has been set to 25, 27, and 29 K subsequently resulting in a lower detection limit between 6.5 and 8.7 nm. Above 25 nm the FCPC reached 96–97% counting efficiency compared to an electrometer used as reference instrument. The FCPC demonstrated its ability to perform continuous measurements over a few hours in the laboratory considering the total particle counting. The instrument will be implemented into the airborne measurement platform ACTOS to perform measurements in the atmospheric boundary layer. Thus, stable operation over 2 h is required and has been demonstrated in the laboratory. The response time of the new FCPC has been estimated in two ways using a time series with highly fluctuating particle number concentrations. The analysis of a sharp ramp due a concentration change results in a response time of 16 ms while a spectral analysis of this time series demonstrates that for frequencies up to 20 Hz coherent structures can be resolved.

1 Introduction

Condensation Particle Counter (CPCs) are the most widely used instruments for measuring submicrometer aerosol particle number concentrations. Inside the CPC, particles which are too small to be detected by direct optical means, grow due to condensation of a working fluid. Afterwards, they are detected by a laser-photodiode optics. Generally, there are three types of CPCs: (1) adiabatic expansion, (2) conductive cooling or continuous flow, and (3) mixing type (Baron and Willeke, 2001). In atmospheric research, the continuous flow type CPC is most frequently used, because of its robustness and reliability. The typical temporal resolution of such CPCs is on the order of

AMTD
3, 5907–5931, 2010

seconds (Quant et al., 1992; Buzorius, 2001; Held and Klemm, 2006). This "low" temporal resolution is caused by the relatively large time required to establish the supersaturation in the laminar flow condenser (Wang et al., 2002). Further delay is caused by zones of recirculation, which leads to a smearing of the number concentration signal.

In atmospheric science, many open questions about particle dynamics require highly time-resolved particle measurements. The spectrum covers vertical turbulent particle fluxes (e.g., the covariance of the vertical velocity and aerosol number concentration), thin stratified layers of increased particle number concentrations, as well as new particle formation due to nucleation and growth connected with turbulent mixing. Enhanced concentrations of small particles have been observed around clouds (Hoppel et al., 1994; Weber et al., 2001) or around the inversion layer due to mixing processes (Stratmann et al., 2003; Siebert et al., 2004). All these phenomena can occur on small spatial scales or are based on atmospheric fluctuations due to the turbulence of the underlaying velocity field (Wehner et al., 2010).

Although ground-based measurements of atmospheric particle fluxes have been reported in the past (Buzorius et al., 1998, 2001; Held and Klemm, 2006; Klemm et al., 2006), measurements with higher temporal resolution are required to resolve the high frequency part of the covariance. In previous experiments, this high frequency part has been ignored leading to an underestimation of the vertical aerosol flux. This is also true in particular for airborne measurements where the requirements for the sampling frequency is even higher to resolve small structures. Nucleation around clouds was mainly observed by fast-flying aircrafts (Weber et al., 2001); with a time resolution in the order of one second the spatial resolution results from the true air speed of the aircraft ($\sim$100 m s^{-1}) to be 100 m. New particle formation may be a locally restricted phenomenon and thus, aircrafts observe a few measurement points only in the region where new particles were formed.

Airborne particle measurements with a higher spatial resolution can be achieved by two ways: (1) reduction of the true airspeed (TAS) of the aircraft, (2) development of faster instrumentation. The first option has already been realized by choosing

AMTD
3, 5907–5931, 2010

a helicopter operating with a TAS of 20 m s^{-1}, which improves the spatial resolution by a factor of five compared with a typical research aircraft with a typical TAS of ≈100 m s^{-1}.

To increase the temporal resolution of aerosol measurements, the development of so-called "mixing-type CPCs" has been started in the eighties (Okuyama et al., 1984). In these instruments, a cold aerosol flow is mixed with a warmer saturated gas flow. In a demonstration study, Wang et al. (2002) showed that mixing times as small as 0.06 s can be achieved with a new design, which is at least 10 times faster than any commercial CPC.

Besides the advantage of having fast mixing-type CPCs as stand-alone instruments, they are also very useful as part of a Scanning Mobility Particle Sizers (SMPS) system, which measures the particle size distribution. The currently used SMPS systems are limited in time resolution to about 45 s (Wang et al., 2002), mainly caused by the slow response of the CPC. With their fast mixing CPC, Wang et al. (2002) have shown that scan times down to 3 s might be possible under certain conditions. However, another limiting factor is the number concentration due to counting statistics, thus atmospheric background measurements will probably not allow scan times shorter than 30 s.

For fast particle measurements the usage of mixing type CPCs has been thus considered and tested in different studies. However, a continuous and stable operation under atmospheric conditions has not been reported yet.

In this investigation, we developed and characterized a new fast mixing-type CPC (FCPC). In contrast to the CPC of Wang et al. (2002), our FCPC is designed for airborne applications in the atmospheric boundary layer. In the following section, we describe the assembly of the FCPC. Thereafter, the dependency of the counting efficiency on the temperature difference between saturator and condenser, its counting stability as well as the time resolution will be presented and discussed.

AMTD
3, 5907–5931, 2010

2 Setup

The fast mixing-type CPC (FCPC) presented here is based on the principle described in Wang et al. (2002) and is shown in Fig. 1. Basically, a warm butanol-saturated air flow is mixed with the aerosol flow within a small mixing volume. Before entering the saturator, the air flow is pressed through a filter and controlled by a needle valve. The saturator contains a wick, which is soaked with liquid butanol during operation. Furthermore, the saturator is equipped with a heating foil and a temperature sensor to provide a defined temperature inside. Similar to Wang et al. (2002), who used a 1/4 inch Swagelok cross in our case a 1/4 inch Swagelok "T" is used as mixing chamber. We tried both options: the Swagelock cross and "T" with similar results. The "T" version was chosen finally, because it saves space in comparison to the cross version. In the following condenser block, the air is cooled causing the required growth of aerosol particles. The Swagelok "T" is isolated and decoupled thermally from the condenser block to avoid cooling of the saturator flow before mixing.

The following condenser block is cooled by a Peltier element and again temperature-controlled by a sensor. The inner diameter of the condenser was decreased to 0.3 mm to minimize the residence time there compared to other CPCs. Because butanol is continuously condensing on the walls of the condenser, a vacuum flow of 0.2 l min^{-1} is connected through a condensation trap to remove any condensed butanol. The butanol droplets are counted in a standard optics from a TSI CPC 3772. The temperatures within the saturator (T_S) and the condenser (T_C) are variable and were changed during the calibration procedure. The reason to do that is to shift the lower measurement limit, i.e. the 50% detection efficiency diameter (D_{P50}).

Aerosol and saturator flow rate of 0.3 l min^{-1} and 0.7 l min^{-1} were found to fulfill the requirements concerning counting statistics, short residence times, and stable operation best. The flows through saturator and optics were adjusted by needle valves and are monitored continuously during operation. The FCPC was designed to be applied at airborne applications, therefore no liquid butanol should be within the instrument,

AMTD
3, 5907–5931, 2010

which is not soaked by the wick. The typical endurance of helicopter-borne measurement flights is usually about 2 h, therefore filling the wick is sufficient and no continuous butanol filling is required. The absence of liquid butanol in the instrument reduces the number of potential wrong countings during flight.

3 Characterization of the FastCPC

3.1 Counting efficiency

The particle counting efficiency curve was determined according to the setup described by Hermann et al. (2007). Here, polydisperse silver aerosol was generated in a tube furnace at temperatures of 1050–1150 °C according to Scheibel and Porstendörfer (1983). Downstream of the furnaces, a dilution system was used to keep the particle number concentration at the CPCs between 1000 and 5000 particles cm^{-3}. This range was chosen in order to have a good signal to noise ratio at the reference electrometer (EM) and to minimize coincidence effects in the CPC optics. After dilution, the aerosol particles were charged in an ^{85}Kr bipolar charger and a monodisperse fraction was selected by a differential mobility analyzer (DMA, Vienna-type, short: L=11 cm, r_{in}=2.5 cm, r_{out}=3.35 cm). The sheath and excess air flow rates of the DMA were adjusted to 20 l min^{-1}, the aerosol and sampling flow rate was set to 2 l min^{-1}. Downstream of the DMA, the monodisperse aerosol was diluted with particle-free air to achieve the required total flow rate for the particle counter(s) and an aerosol electrometer (TSI 3068B) as reference instrument. The EM flow rate was 2 l min^{-1} and the EM data were corrected for background offset, measured regularly between the particle measurements. The individual instruments were fed from a 2 m long tube header with 11 ports downstream the mixing bottle. Sampling lines from the header to the instruments were arranged in a symmetric pattern with a 40 cm straight line each. During our study the temperature in the condenser of the FCPC was kept constant at 10 °C while the saturator temperature was set to 35 °C, 37 °C, and 39 °C.

AMTD
3, 5907–5931, 2010

The counting efficiency was measured for diameters between 5 and 30 nm, the counting time at each selected diameter was 5 min. The calibration curves were measured at least three times for each temperature difference and mean values were calculated. The FCPC particle counting efficiency η was finally calculated as the ratio of the mean FCPC and EM particle number concentrations at each individual particle diameter.

Figure 2 shows the mean values for the FCPC at the three different temperature settings. According to Stolzenburg (1988) the error in diameter accounts for approximately ±0.3–1.3 nm representing one sigma of the DMA transfer function. Uncertainties in the counting efficiency result from the standard deviations of the mean values for each diameter. For the FCPC the standard deviation was usually below 5% of the counting efficiency, but in the slope it can be higher (up to 10%).

The data were fitted using a four-parameter exponential function:

$$\eta = a - \frac{b}{\exp(c \cdot \log(x)) - d}. \quad (1)$$

With the help of this empirical approach, the diameters of the 50% particle detection efficiency, D_{P50}, were calculated. In this context, the D_{P50} was defined as particle diameter where the counting efficiency reaches half the maximum of the reference instrument (100%). The fitting parameters as well as the D_{P50} values are summarized in Table 1. The three curves are similar in shape, those with a higher temperature difference are shifted to smaller diameters as expected from theory (Banse et al., 2001). For the given temperature settings, the D_{P50} varies between 6.5 and 8.7 nm. In general the shape of the curves is similar to other commercial CPCs as presented in Hermann et al. (2007), Petäjä et al. (2006), and Wiedensohler et al. (1997).

3.2 Counting stability

In addition to the size-dependent counting efficiency the measurement stability of a particle counter has to be investigated. The presented FCPC is intended to measure

AMTD
3, 5907–5931, 2010

onboard the helicopter-borne platform ACTOS (Siebert et al., 2006), where measurement flights last typically 2 h. Thus, stable particle counting over this period is required for any deployed instrumentation. To test the stability, various measurements have been performed in the laboratory.

First, the FCPC was operated over few hours parallel with a TSI 3776 under laboratory conditions. Figure 3 shows the evolution of the ratio FCPC/TSI 3776 within 7 h measuring ambient air from the laboratory. The FCPC was operated with $T_S = 37\,^{\circ}C$ and $T_C = 10\,^{\circ}C$ and butanol was filled into the saturator prior to the measurement. In fact, the ratio between both CPCs was stable for 5 h, which is sufficient for the desired flight endurance with an average value of 0.85. Both CPCs have a different D_{P50} but the ratio of the total number concentration should be constant if the fraction of particles between 3 and 7 nm was constant. This should be true, since no source for ultrafine particles was active in the laboratory. The lower graph of Fig. 3 shows the scatter plot of measured number concentrations during 250 min from start. Obviously measurements from both counters are well correlated ($R^2 = 0.98$), the standard deviation from the linear trend is $\sim 19\,cm^{-3}$. After 6 h of continuous operation the counting efficiency dropped significantly caused by the smaller butanol reservoir of the FCPC compared to the TSI 3776.

In addition to the comparison of total number concentrations, the stability at individual particle sizes was investigated. With regard to the counting efficiency curve (Fig. 2), measurements at individual diameters have been performed: (1) diameters on the slope of the counting efficiency curve (close to D_{P50}), to check how stable the location of this slope is, (2) diameters above the slope, i.e. where the counting efficiency reached its maximum value.

Figure 4 shows the ratio of number concentrations measured by FCPC and EM measuring 8-nm silver particles over 2 h. The FCPC was operated at $T_S|T_C = 37\,^{\circ}C|10\,^{\circ}C$. Consequently 8 nm correspond to the steep part of the counting efficiency curve ($\eta \approx 0.6$, cf. Fig. 2). The ratio decreased during that time by approximately 0.08, in the figure a linear trend is fitted to the data. Further measurements with diameters on

AMTD
3, 5907–5931, 2010

the steep part of the slope gave a similar picture. This decrease in counting efficiency is probably due to the decreasing butanol reserve within the saturator of the FCPC. Thus, either the decreasing butanol reserve decreases the counting efficiency in general or it shifts only the 50%-detection efficiency diameter towards larger diameters. To prove this, measurements at 30 nm were performed, where the counting efficiency is at its maximum value.

Figure 5 shows the ratio of number concentrations measured by the FCPC and the EM for 30-nm silver particles (upper plot), and the corresponding scatter plot of the absolute concentration values (lower plot). The FCPC was operated again at $T_S|T_C = 37\,^{\circ}\mathrm{C}|10\,^{\circ}\mathrm{C}$. The mean ratio is stable over 6 h and a trend is not recognizable. The lower plot illustrates that both measurements are well correlated ($R^2 = 0.94$), the standard deviation from the linear trend is 81 cm^{-3}.

Finally, from the stable ratio at 30 nm one can conclude that the counting efficiency does not decrease in general with decreasing butanol content in the saturator within the first hours after filling. The decrease in counting efficiency is limited to diameters on the slope around D_{P50}, largest effects occur from 6 to 12 nm. Thus the counting efficiency curve moves to a slightly larger particle size when the butanol reserve decreases. A decrease of 10% at a fixed size on the slope, which was observed for 8-nm particles corresponds to a shift of less than 0.5 nm, which is within the uncertainty of the curve.

3.3 Time response: experiments under atmospheric conditions

The time response of CPCs was investigated in previous studies by different techniques such as applying fast valves in laboratory setups (e.g., Held and Klemm, 2006) or performing measurements under atmospheric conditions analyzing the statistical behavior of natural fluctuations of particle concentrations due to atmospheric turbulence (Buzorius, 2001).

Our approach is taking advantage of the combination of atmospheric turbulence near ground and a strong isolated particle source, which results in strong fluctuations due to the sharp gradients in the particle number concentration. Such strong gradients are

AMTD
3, 5907–5931, 2010

usually not observed in the atmosphere but the resulting conditions provide a perfect laboratory to estimate the time response of the new FCPC. The following analysis is two-folded: (i) the structure of a sharp ramp is analyzed to estimate the typical time response and (ii) power spectral analysis is used to distinguish between coherent structures in a turbulent flow field and the white noise of purely Poisson distributed particle concentration. Coherent structures will result in a spectrum with a slope of approximately "−5/3" (so-called "inertial subrange behavior"), whereas white noise will result in a flat spectrum. The latter can be due to increasing sampling noise which means that not enough particles are counted (very unlikely for our experiment) or that the time response of the FCPC is to low to resolve the coherent structures. Therefore, the transition region between the inertial subrange and white noise can be used to estimate the time response of the FCPC.

3.3.1 Time series analysis

Figure 6 shows a 800-s long record of the particle number concentration N measured with the FCPC under atmospheric conditions. The FCPC was placed in a height of ∼1 m above ground, a gasoline power generator was running as a particle point source 5 m upstream of the measurement location. The mean wind speed was about 2–3 m s^{-1} with slightly varying direction. The sampling gate of the data acquisition system was set to 10 ms which implies a sampling frequency of 100 Hz.

The time series indicates strong fluctuations of N representing the coherent structures of the turbulent wind field. The amplitude of N ranges from about 1 to 3×10^4 cm^{-3} for the atmospheric background superimposed by concentrations of up to 8×10^4 cm^{-3} representative for the exhaust of the power generator.

A 25-s long subrecord is shown in the lower panel and highlights the sharp ramp structures at the edges of the "exhaust events". Such sharp ramps will now be used to estimate the typical time response of the FCPC.

It is widely common to describe the temporal behavior of a CPC as a "first-order response system", which means the change of the measured concentration dN/dt is

AMTD
3, 5907–5931, 2010

proportional to the concentration N which results in a solution for $N(t)$ such as:

$$N_i(t) = N_0(t_0) \cdot \exp\left(\frac{t - t_0}{\tau}\right), \quad (2)$$

where N_0 is the true ambient concentration at time t_0, N_i the concentration measured by the CPC, and τ the response time.

Figure 7 shows a 120-ms long subrecord including a sharp ramp which was marked by the blue box in Fig. 6. The change of the particle number concentration δN is about $6 \times 10^4\,\mathrm{cm}^{-3}$; the horizontal dashed line in Fig. 7 indicates the concentration where $1-1/e$ of δN (i.e., $N_0 + 63\%$ of δN) is reached. From this plot we estimate the e-folding time $\tau \approx 16$ ms as the response time of the FCPC. The response time for CPC TSI 3010 was measured in different studies and is between 0.77 and 0.96 s (Buzorius, 2001; Held and Klemm, 2006), which is approximately a factor of 50 higher.

3.3.2 Spectral behavior

In order to distinguish between the coherent structures in the turbulent concentration field and white noise of purely Poisson distributed particles spectral analysis is applied. From the time series of N presented above power spectral density functions (hereafter called "spectra") are estimated by using a Fast Fourier Transformation (FFT). That is, the variance of N per frequency interval is displayed as a function of frequency f. From turbulence theory we know that the spectrum of a turbulent time series results in a spectrum which scales approximately with $f^{-5/3}$ in the so-called inertial subrange. This inertial subrange is from about a few millimeters up to the largest eddies in the atmosphere and we can safely conclude that our particle measurements are well within the inertial subrange for frequencies above ~0.5 Hz which means eddies of the size of about 4–5 m and less.

Figure 8 shows the spectra of N in a log-log representation; the dashed line indicates the −5/3 slope as a reference for inertial subrange scaling. The red and black curve represents the spectra of the complete record. The black spectrum curve is with full

AMTD
3, 5907–5931, 2010

resolution (100 Hz) and for the red curve an non-overlapping average of two samples is applied to reduce the noise at the high-frequency end of the spectrum. The blue spectrum is for a 300-s long subrecord (t=150–400 s) with less fluctuations and more stationary conditions (see Fig. 6).

All spectra follow the −5/3 slope in the range between 0.5 and 3 Hz, for higher frequencies up to ∼20 Hz the spectra drop off until the spectra begin to flatten (most obvious for the blue curve). The drop-off is most likely due to a low-pass filtering effect which results from mixing inside the FCPC. This mixing smears out structures resulting in a steeper slope compared with inertial subrange scaling. Measurements of spatial scales smaller than a typical dimension D of the measurement system itself will be influenced by this averaging. As a simple assumption, this averaging can be approximated by a running mean with a window width D which results in a spectral transfer function which deviates from one at spatial scales smaller than $L \approx \pi \cdot D$. For our setup $D = 20$ cm (distance from the inlet to the optical device) is a rough approximation resulting in $L = 60$ cm. This agrees well with our observation where the spectrum shows a deeper slope at a scale $\sim 2\,\mathrm{m\,s^{-1}}/3\,\mathrm{Hz} \approx 60$ cm.

The flatten at the high-frequency end of the spectrum is due to the increasing influence of white noise. For comparison, the spectrum of purely Poisson distributed data (e.g., white noise) is shown (green curve); the spectrum of white noise is flat as expected for uncorrelated data.

Summarizing, power spectral analysis of the whole record suggests that the signal of the FCPC is still not complete noisy (e.g. flat) at the maximum frequency of 50 Hz which means that the response time is better than 20 ms. This observation agrees with the estimated e-folding time of 16 ms from the analysis of the ramp structure.

4 Summary and outlook

A new mixing-type CPC has been built based on the setup of Wang et al. (2002). The time resolution of this instrument is significantly higher than that of commercially

AMTD
3, 5907–5931, 2010

available instruments, therefore it is called FastCPC (FCPC). The functionality and stable operation of the FCPC was demonstrated in the laboratory as well as under atmospheric conditions for the first time.

The counting efficiency shows a similar behavior than laminar flow-type CPCs: with increasing temperature difference the slope is moving to smaller diameters. Here, temperature differences from 25 to 29 K were chosen leading to a D_{P50} between 6.5 and 8.7 nm. Above 25 nm the counting efficiency reached its maximum value of 96–97% compared to the electrometer, which is similar to other commercial CPCs. The FCPC demonstrated its ability to perform stable measurements over few hours, only the slope of the counting efficiency curve is moving to larger particle sizes when no butanol is filled continuously. A decrease of 10% at a fixed size on the slope corresponds to a shift of less than 0.5 nm, which is within the uncertainty of the curve. Considering the total number concentration only the shift is negligible. For potential ground-based or long-term applications the FCPC needs to be modified to ensure a continuous butanol supply into the wick. As proposed, the current version fulfills the requirements of a two-hour measurement flight of the helicopter-borne platform ACTOS.

The response time was estimated using a combination of atmospheric turbulence and an artificial aerosol source creating sharp gradients in the particle number concentration. Under these conditions a response time of 16 ms was found, which is a factor of 50 below that of most commercially available laminar flow-type CPCs (e.g. TSI 3010).

However, averaging effects inside the FCPC influence the measurements of spatial scales comparable to the system dimension. Spectral analysis shows therefore a drop-off compared with classical turbulence theory at a spatial scale of about 60 cm. At the maximum observed frequency of 50 Hz, the signal of the FCPC is still not complete noisy meaning that the response time of the current version of the FCPC is better than 20 ms. This in in good agreement with the analysis of the ramp structure showing a response time of 16 ms.

In the next step the new FCPC will be implemented on the helicopter-borne platform ACTOS and applied in boundary layer measurements. The focus will be the analysis

AMTD
3, 5907–5931, 2010

of particle number fluctuations in regions with highly turbulent structures such as cloud edges and mixing zones near inversions. The FCPC enables airborne particle measurements on the meter-scale for the first time which will improve the understanding of small-scale processes significantly.

Acknowledgements. The authors thank Michael Eckinger and Christian Kraft for their assistance in the laboratory, i.e. the calibration and modification of different versions of the FCPC. The project was supported by the German Science Foundation DFG (WE 2757/1-1).

References

Banse, D. F., Esfeld, K., Hermann, M., Sierau, B., and Wiedensohler, A.: Particle counting efficiency of the TSI CPC 3762 for different operating parameters, J. Aerosol Sci., 32, 157–161, 2001. 5913

Baron, P. A. and Willeke, K.: Aerosol Measurements: Principles Techniques and Applications, John Wiley and Sons, New York, 1131 pp., 2001. 5908

Buzorius, G., Rannik, Ü., Mäkelä, J. M., Vesala, T., and Kulmala, M.: Vertical aerosol particle fluxes measured by eddy covariance technique using condensational particle counters, J. Aerosol Sci., 129, 157–171, 1998. 5909

Buzorius, G.: Cut-off sizes and time constants of the CPC TSI 3010 operating at 1–3 lpm flow rate, Aerosol Sci. Technol., 35, 577–585, 2001. 5909, 5915, 5917

Buzorius, G., Rannik, Ü., Nilsson, D., and Kulmala, M.: Vertical fluxes and micrometeorology during aerosol particle formation events, Tellus B, 53, 394–405, 2001. 5909

Held, A. and Klemm, O.: Direct measurement of turbulent particle exchange wit a twin CPC eddy covariance system, Atmos. Environ., 40, S92–S102, 2006. 5909, 5915, 5917

Hermann, M., Wehner, B., Bischof, O., Han, H.-S., Krinke, T., Liu, W., Zerrath, A., and Wiedensohler, A.: Particle counting efficiencies of new TSI condensation particle counters, J. Aerosol Sci., 38, 374–682, 2007. 5912, 5913

Hoppel, W. A., Frick, G. M., Fitzgerald, J. W., and Laerson, R. E.: Marine boundary layer measurements of new particle formation and the effects nonprecipitating clouds have on aerosol size distribution, J. Geophys. Res., 99, D7, 14443–14459, 1994. 5909

Klemm, O., Held, A., Forkel, R., Gasche, R., Kanter, H. J., Rappenglueck, B., Steinbrecher, R.,

AMTD
3, 5907–5931, 2010

Müller, K., Plewka, A., Cojocariu, C., Kreuzwieser, J., Valverde-Canossa, J., Schuster, G., Moortgat, G. K., Graus, M., and Hansel, A.: Experiments on forest/amtosphere exchange: climatology and fluxes during two summer campaigns in NE Bavaria, Atmos. Environ., 40, S3–S20, 2006. 5909

Okuyama, K., Kousaka, Y., and Moutouchi, T.: Condensational growth of ultrafine aerosol-particles in a new particle-size magnifier, Aerosol Sci. Tech., 3, 353–366, 1984. 5910

Petäjä, T., Mordas, G., Manninen, H., Aalto, P. P., Hämeri, K., and Kulmala, M.: Detection efficiency of a water-based TSI condensation particle counter 3785, Aerosol Sci. Tech., 40, 1090–1097, 2006. 5913

Quant, F. R., Caldow, R., Sem, G. J., and Addison, T. J.: Performance of condensation particles counters with three continuous-flow designs, Aerosol Sci. Tech., 23, S405–S408, 1992 5909

Scheibel, H. G. and Porstendörfer, J.: Generation of monodisperse Ag- and NaCl aerosols with particle diameters between 2 and 300 nm, J. Aerosol Sci., 14, 113–126, 1983. 5912

Siebert, H., Stratmann, F., and Wehner, B.: First observations of increased ultrafine particle number concentrations near the inversion of a continental planetary boundary layer and its relation to ground-based measurements, Geophys. Res. Lett., 31, L09102, doi:10.1029/2003GL019086, 2004. 5909

Siebert, H., Franke, H., Lehmann, K., Maser, R., Saw, E. W., Schell, D., Shaw, R. A., and Wendisch, M.: Probing fine-scale dynamics and microphysics of clouds with helicopter-borne measurements, B. Am. Meteorol. Soc., 87, 1727–1738, 2006. 5914

Stolzenburg, M. R.: An ultrafine aerosol size distribution measuring system, Ph.D. thesis, Mechanical Engineering Department, University of Minnesota, Minneapolis, USA, 1988. 5913

Stratmann, F., Siebert, H., Spindler, G., Wehner, B., Althausen, D., Heintzenberg, J., Hellmuth, O., Rinke, R., Schmieder, U., Seidel, C., Tuch, T., Uhrner, U., Wiedensohler, A., Wandinger, U., Wendisch, M., Schell, D., and Stohl, A.: New-particle formation events in a continental boundary layer: first results from the SATURN experiment, Atmos. Chem. Phys., 3, 1445–1459, doi:10.5194/acp-3-1445-2003, 2003. 5909

Wang, J., McNeill, V. F., Collins, D. R., and Flagan, R. C.: Fast mixing condensation nucleus counter: Application to rapid scanning differential mobility analyzer measurements, Aerosol Sci. Tech., 36, 678–689, 2002. 5908, 5909, 5910, 5911, 5918

Weber, R. J., Chen, G., Davis, D. D., Mauldin III, R. L., Tanner, D. J., Eisele, F. L., Clarke, A. D., Thornton, D. C., and Bandy, A. R.: Measurements of enhanced H_2SO_4 and 3–4 nm particles near a frontal cloud during First Aerosol Characterization Experiment (ACE 1), J. Geophys.

AMTD
3, 5907–5931, 2010

Res., 106, D20, 24107–24117, 2001. 5909
Wehner, B., Siebert, H., Ansmann, A., Ditas, F., Seifert, P., Stratmann, F., Wiedensohler, A., Apituley, A., Shaw, R. A., Manninen, H. E., and Kulmala, M.: Observations of turbulence-induced new particle formation in the residual layer, Atmos. Chem. Phys., 10, 4319–4330, doi:10.5194/acp-10-4319-2010, 2010. 5909
Wiedensohler, A., Orsini, D., Covert, D. S., Coffman, D., Cantrell, W., Havlicek, M., Brechtel, F. J., Russell, L. M., Weber, R. J., Gras, J., Hudson, J. G., and Litchy, M.: Intercomparison study of the size-dependent counting efficiency of 26 condensation particle counters, Aerosol Sci. Tech., 27(2), 224–242, 1997. 5913

AMTD
3, 5907–5931, 2010

Table 1. Fit parameters a, b, c, and d for Eq. (1) as well as the 50% detection diameter D_{P50} of the mean FCPC counting efficiency curves as presented in Fig. 2.

T_S (°C)	T_C (°C)	a	b	c	d	D_{P50} (nm)
39	10	0.961	154.83	7.36	55.52	6.5
37	10	0.975	34.70	5.22	21.35	7.5
35	10	0.965	61.92	5.46	33.84	8.7

AMTD
3, 5907–5931, 2010

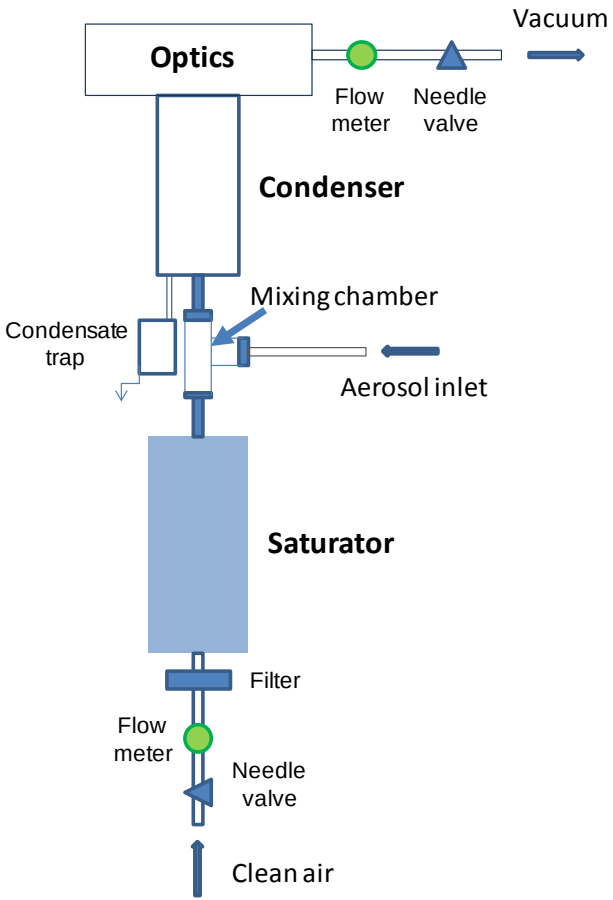

Fig. 1. Schematic of the new FastCPC. A warm butanol-saturated air flow is mixed with the aerosol flow inside a Swagelok "T". In the following condenser block the air is cooled, causing the required growth of aerosol particles to be counted inside the optics.

AMTD
3, 5907–5931, 2010

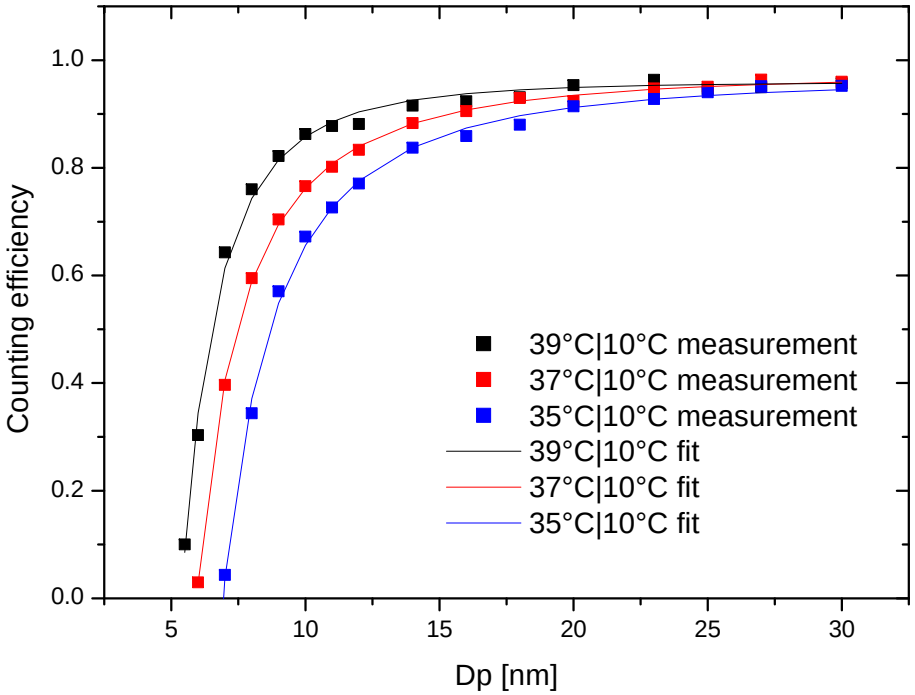

Fig. 2. Counting efficiency of the Fast CPC at different temperature differences compared to the electrometer (TSI 3068B). Quadrates present the mean measurement points, the solid lines are fitted using Eq. (1). The corresponding fit parameters as well as the 50% detection diameter D_{P50} are given in Table 1.

AMTD
3, 5907–5931, 2010

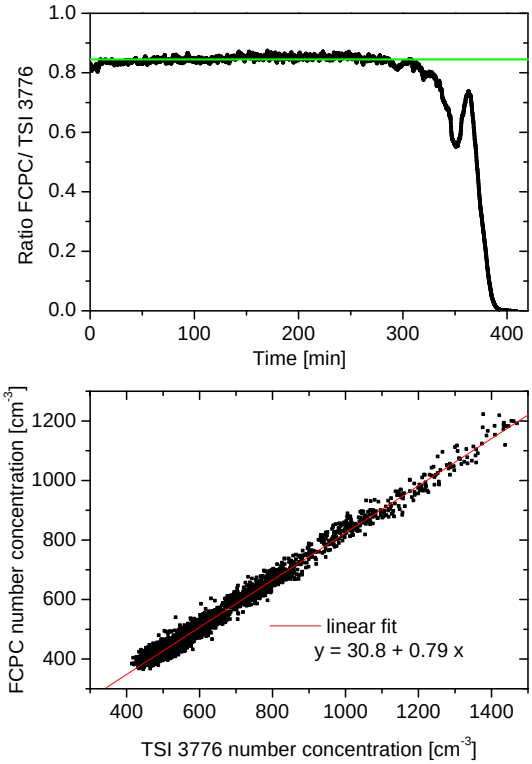

Fig. 3. Comparison of FCPC and TSI 3776 sampling room air from the laboratory. The upper plot displays the time series of the ratio number concentrations FCPC/TSI 3776. The horizontal green line displays the average value (0.85) during 250 min from start. The lower plot shows the direct comparison of the number concentration measurement for these 250 min from start as well as a linear fit.

AMTD
3, 5907–5931, 2010

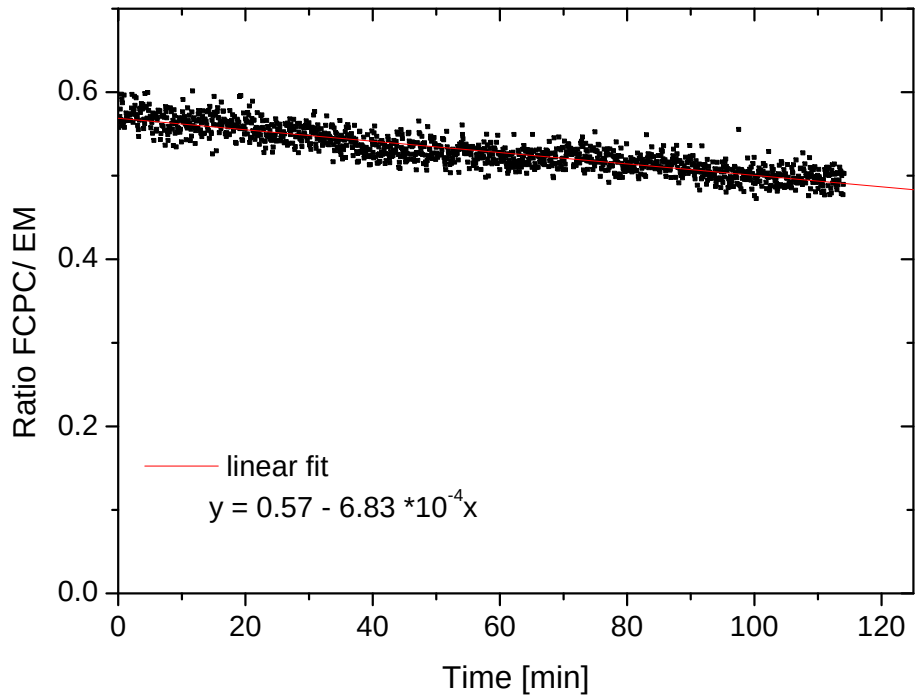

Fig. 4. Counting efficiency of the FCPC in comparison with the electrometer (ratio FCPC/EM) measuring 8-nm silver particles at 37 °C|10 °C. The red line displays the linear trend.

AMTD
3, 5907–5931, 2010

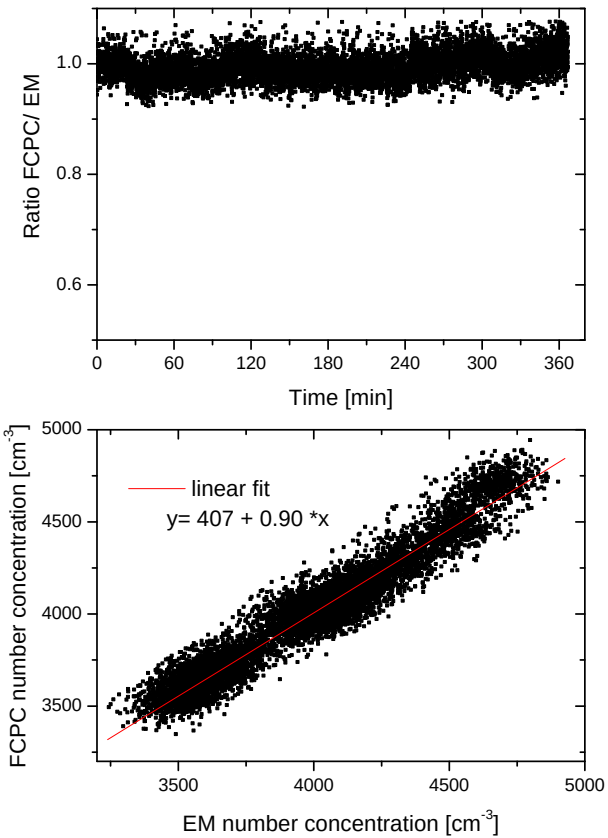

Fig. 5. Counting efficiency of the FCPC in comparison with the electrometer (ratio FCPC/EM) measuring 30-nm silver particles at 37˚C|10˚C: the upper plot shows the ratio FCPC/EM, the lower one the corresponding scatter plot of the number concentrations. The red line displays the linear trend in the lower plot.

AMTD
3, 5907–5931, 2010

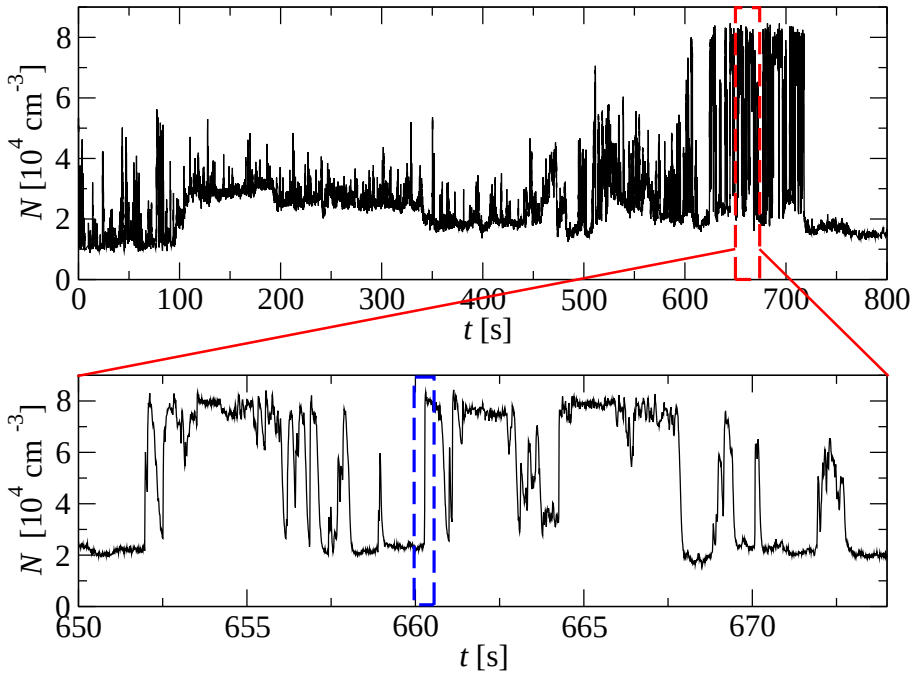

Fig. 6. Time series of particle number concentration N measured with the FCPC under atmospheric conditions, about 5 m downstream of an artificial particle source (gasoline power generator). The sampling gate was 10 ms. At the end of the record (t ~600–720 s), the power generator was running out of gasoline resulting in an increased production of particles. The lower panel shows an enlarged portion of the record with strong variation of N due to the fluctuations of the wind direction and the particle production of the power generator. The blue box depicts a sharp ramp analyzed in Fig. 7.

AMTD
3, 5907–5931, 2010

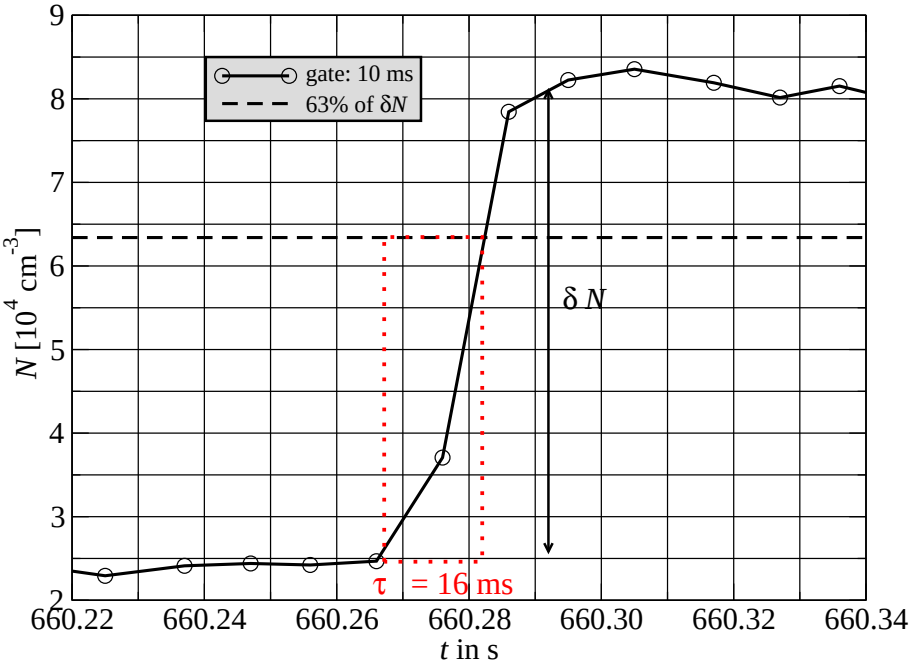

Fig. 7. A 120-ms long subrecord of the time series presented in Fig. 6 marked by the blue box is shown. The varying wind direction created strong fluctuations of N resulting in sharp ramps. Assuming a first-order response of the FCPC, the e-folding time τ can be estimated from such a ramp to $\tau \approx 16$ ms.

AMTD
3, 5907–5931, 2010

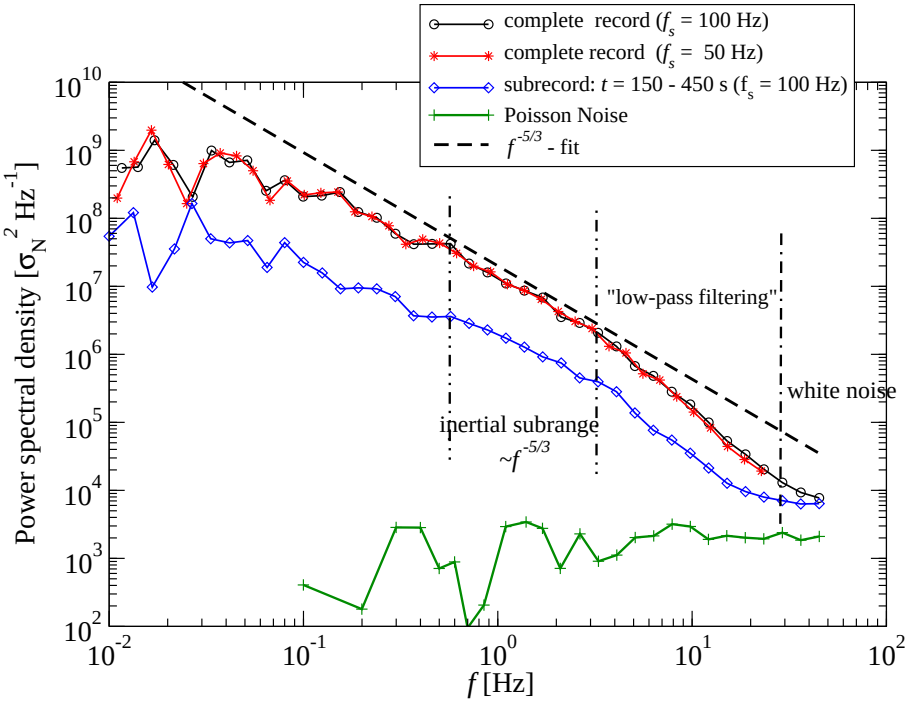

Fig. 8. Power spectral density functions of the complete record (see Fig. 6) are shown (black and red curves) and of a 300-s long subrecord (blue curve). The green curve shows the spectral density of Poisson distributed data resulting in white noise (flat line). The black dashed line indicates a −5/3 slope for inertial subrange scaling.

AMTD
3, 5907–5931, 2010